Electronic Supplementary Information

Fe-doping into NiTe bulk crystal as a robust catalyst for electrochemical oxygen evolution reaction

Lei Zhong, Yufei Bao, Xu Yu and Ligang Feng*

School of Chemistry and Chemical Engineering, Yangzhou University, Yangzhou 225002, P.R. China.

Email: ligang.feng@yzu.edu.cn; fenglg11@gmail.com (L Feng*)

Experimental Section

Chemicals

All chemicals were purchased and used without further purification. Tellurium dioxide (TeO_2), Triethylene glycol (TEG), Oleylamine (OAm) and Ethylene glycol ($C_2H_6O_2$, AR) were bought from Shanghai Aladdin Bio-Chem Technology Co., LTD. Potassium hydroxide (KOH, AR), Nickel(II) Chloride Hexahydrate Puratrem ($NiCl_2 6H_2O$), hexane and ferric chloride hexahydrate ($FeCl_3 6H_2O$) were purchased from Sinopharm Chemical Reagent Co., Ltd. Polyvinylpyrrolidone (PVP) (M_w=40000) were obtained from Energy Chemical. L-ascorbic acid was purchased from Shanghai Macklin Biochemical Co, Ltd. All solutions were prepared with ultrapure water (Thermo Fisher Scientific (USA) Co., Ltd).

Catalyst fabrication:

Synthesis of Te

0.168 g TeO_2, 0.1675 g KOH and 30 mL TEG were added into a three-necked flask under magnetic stirring at 85 ^oC for 10 min to form a homogeneous solution. Subsequently, 0.45 g L-ascorbic acid and 0.1 g PVP were added with continuous stirring for 10 min. The obtained solution was transferred into a 100 mL Teflon-lined stainless steel autoclave, sealed and reacted at 150 ^oC for 6 h. Finally, the product was precipitated using acetone, cleaned with DI water and dried overnight in a vacuum oven at 60 ^oC.

Synthesis of Fe-NiTe catalysts

Fe doped NiTe nanocrystals with different concentrations were synthesized according to the following procedures. 4 mmol Te was dispersed in 5 mL TEG in a three-necked flask under magnetic stirring. And then, 4 mmol $NiCl_2{\cdot}6H_2O$ and 0.8 mmol $FeCl_3 6H_2O$ were added into the solution. After that, the solution was heated to 110 ^oC at a heating rate of 10 ^oC min^{-1} and kept for 1 h under N_2 atmosphere. And then 0.5 mL OAm was injected into the solution. The mixture solution was then heated to 220 ^oC at a heating rate of 10 ^oC min^{-1} and kept for 80 min. After cooling to room temperature, the black precipitate was washed with ethanol, hexane, and dried at 60 ^oC for 12 h.

The as-obtained product was denoted as Fe-NiTe-2. For comparison, Fe-NiTe-1 and Fe-NiTe-3 were synthesized according to the same procedure except for the amount of 0.6 mmol and 1.0 mmol $FeCl_3$ $6H_2O$ employed, respectively.

Characterization

The sample was characterized on Bruker D8 advance X-ray diffraction (XRD) with Cu Kα radiation source operating at 40 kV and 40 Ma at a scanning rate of 5°/min. The morphology and microstructure were examined with a transmission electron microscopy (TEM, Philips, TECNAI 12, Holland). Energy X-ray detector spectrum (EDS) images were obtained on a TECNAI G2 F30 transmission electron microscope (acceleration voltage: 300 kV). High-resolution TEM and Energy-dispersive X-ray spectroscopy (EDX) mapping images were taken under a scanning TEM modal. X-ray photoelectron spectroscopy (XPS) measurement was carried out on an ECSALAB250Xi spectrometer with an Al Kα radiation source.

Electrochemical measurements

All the electrochemical measurements were carried out by a conventional three-electrode system via a Bio-Logic VSP electrochemical workstation (Bio-Logic Co, France). The working electrode was prepared by coating the catalyst ink over the glassy carbon electrode (3 mm diameter, 0.07 cm^{-2}). The graphite rod and the saturated calomel electrode (SCE) served as the counter and reference electrode, respectively. Notably, the SCE was calibrated before and after the tests to make sure the accuracy. All potential was converted and referred to a reversible hydrogen electrode (RHE), E(RHE) = E(SCE)+ 0.059*pH+ 0.24 V. According to the equation ($E_{calibration} = E_{original} - iR_s$), the iR correction was done to offset the uncompensated solution resistance (R_s) and the uncompensated solution resistance was measured to be 8 Ω by electrochemical impedance and 80% of the resistance was compensated.

The catalyst ink was prepared as follows: The as-obtained catalysts (5mg) were uniformly dispersed in the mixed solution of 950 μL absolute ethyl alcohol and 50 μL Nafion solution (5wt.%) through the sonication for 1 h. Then 10 μL of the catalyst ink was pipetted and dropped onto the center of a pre-cleaned glassy carbon and dried naturally. The glassy carbon electrode was pre-

cleaned by with alumina slurry of 50 nm, ethanol and water; and finally dried at the room temperature before using. For OER tests, the linear sweep voltammograms (LSV) and cyclic voltammograms (CV) were measured at a scan rate of 5 mV s^{-1} in 1 M KOH solution. The 1 M KOH solution was purged by pure N_2 for approximately 30 min. For comparions, the 1 M KOH solution saturated by pure O_2 for 30 min was also compared for the OER measurements on Fe-NiTe-2 electrode. Fe-containing electrolyte was obtained from the fresh electrolyte after long-term stability test of Fe-NiTe-2, in which Fe was dissolution into the KOH solution.

Tafel analysis

For the Tafel equation, $\eta = a + b \log (j)$, where η (V) is the overpotential, j (mA cm^{-2}) is the current density and b (mV dec^{-1}) represented the Tafel slope.

ECSA measurement and calculation

The electrochemical active surface area (ECSA) was evaluated in terms of doubler layer capacitance (C_{dl}). The ECSA was estimated by cyclic voltammetry without Faradaic processes occurred region from 0.73 V to 0.83 V in 1 M KOH at scan rates were 20, 40, 60, 80, 100 mV s^{-1}. The C_{dl} was estimated by plotting j at 0.78 V vs. RHE (where j is the current density) against the scan rate. The electrochemical active surface area is evaluated for a flat surface by assuming 40 μF cm^{-2} according to previous literature [1]

Electrochemical Impedance Measurements

The electrochemical impedance spectroscopy (EIS) was recorded in the above three-electrode cell at room temperature in 1M KOH and the frequency varied from 1000 kHz to 10 mHz.

Stability test and Chronoamperometry measurement

The dynamical stability was tested for 1000 cycles at the constant scan rate of 50 mV s^{-1}. After 1000 cycles, the stable polarization curve was recorded for comparison with the initial curve. To estimate the stability of the catalysts, the chronoamperometry was also performed in 1M KOH solution at a fixed potential of 1.52 V vs. RHE for 12 h.

Specific activity and Turnover of frequency (TOF) calculation

The specific activity was obtained by normalizing the apparent current to ECSA. The TOF (s^{-1}) for OER can be calculated with the following equation TOF (s^{-1}) = I / (4* F* n), Where I is the

current (A) during linear sweep measurement, F is the Faraday's constant (96485.3 C/mol), n is the number of active sites (mol).[2-4]

Faradaic yield test

The working electrode was prepared by drop-casting catalyst suspension on the glassy carbon electrode with the surface area of 0.07 cm^{-2}. A constant potential of 1.52 V vs. RHE for OER was applied on the electrode and evolved gas was continually recorded. Thus, the faradaic yield was calculated from the ratio of the recorded gas volume to the theoretical gas volume during the charge passed through the electrode.

$$\text{Faradaic yield} = V_{experimental}/V_{theoretical} = V_{experimental}/ (1/4 \times Q/ F \times V_m)$$

where Q is the charge passed through the electrode, F is Faraday constant (96485 C mol^{-1}), the number 4 means 4 mole electrons per mole O_2, the number 1 means 1 mole O_2, V_m is molar volume of gas (24.5 L mol^{-1}, 298 K, 101 KPa).

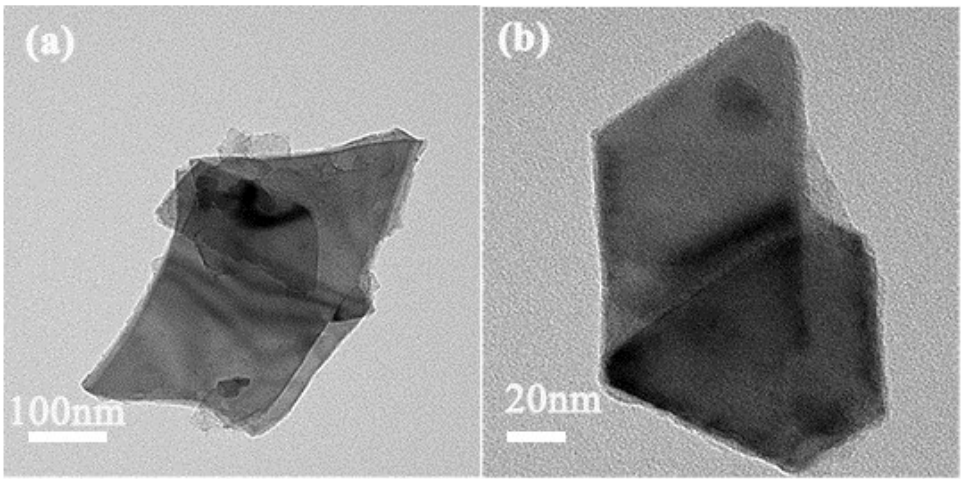

Fig. S1 TEM images (a, b) of Fe-NiTe-2 catalyst.

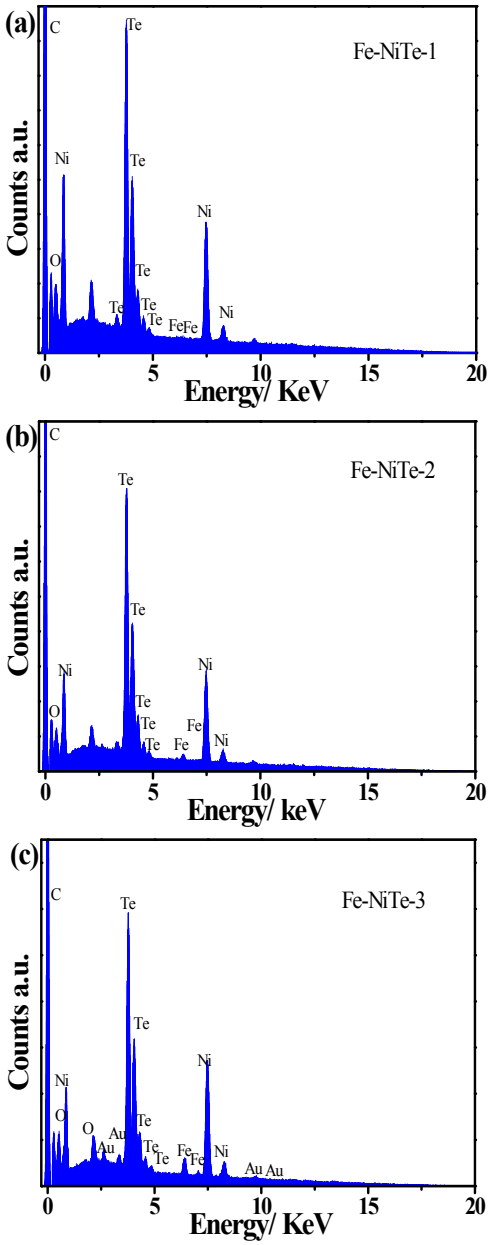

Fig. S2 EDS spectra of (a) Fe-NiTe-1, (b) Fe-NiTe-2 and (c) Fe-NiTe-3 catalysts.

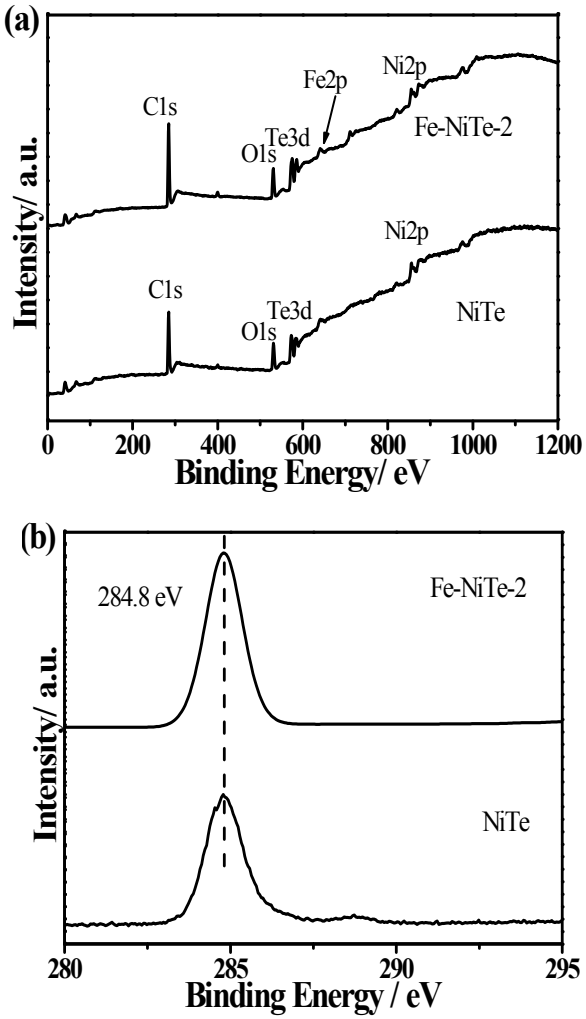

Fig. S3 XPS survey spectrum (a) and high resolution XPS spectra of C1s (b) of NiTe and Fe-NiTe-2. The peak of C 1s at 284.8 eV was used as references to calibrate all the peaks position.

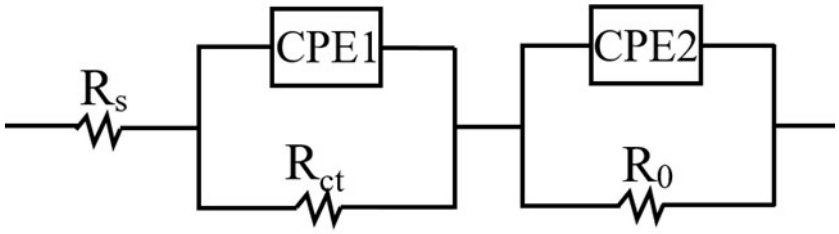

Fig. S4 EIS fitting equivalent circuit of Nyquist plots for NiTe and Fe-doped NiTe catalysts.

The equivalent circuit includes a parallel combination of (R_{ct}, CPE1) and (R_0, CPE2) element in series with R_s. The constant phase angle element (CPE) generally was employed to well fit the impedance data by safely treating as an empirical constant without considering the its physical basis. And mostly, it was regarded as the double layer capacitor from the catalyst/support and catalyst solution. R_s was a sign of the uncompensated solution resistance, R_{ct} was a charge transfer resistance arisen from the relevant electro-chemical oxidation, R_0 was associated to the contact resistance between the catalyst material and the others resistance.

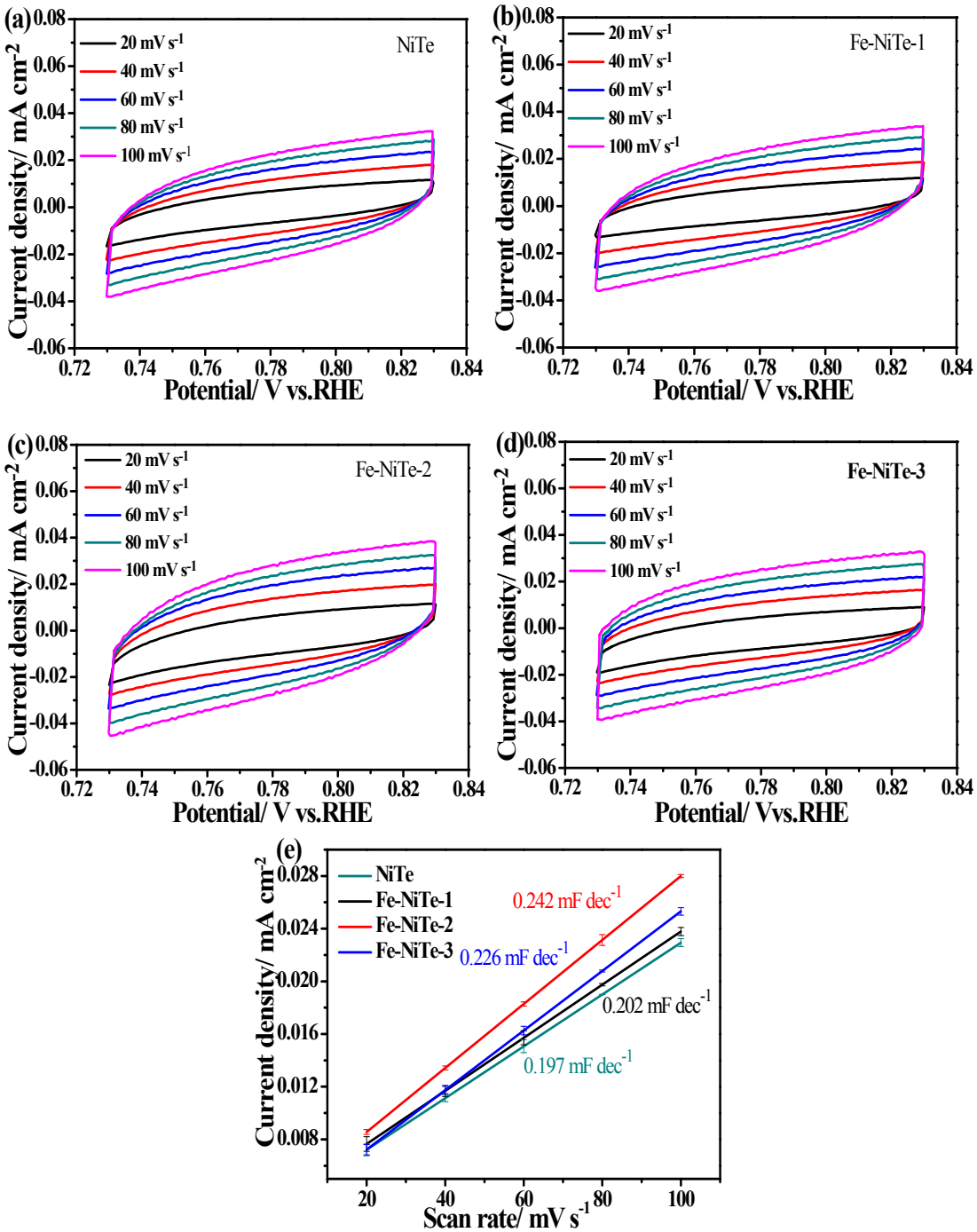

Fig. S5 Cyclic voltammograms (a, b, c and d) and double layer capacitance (e) of NiTe and Fe-doped NiTe catalysts. The capacitive currents as a function of scan rate ($\Delta j = (j_a - j_b)/2$). C_{dl}: doubler layer capacitance; ECSA: electrochemical active surface area.

The open-circuit potential (OCP) of NiTe and Fe-NiTe-1, Fe-NiTe-2, Fe-NiTe-3 are 0.787, 0.775, 0.780, 0.783 V vs. RHE, which falls into the nonfaradaic potential range used for the C_{dl} calculation

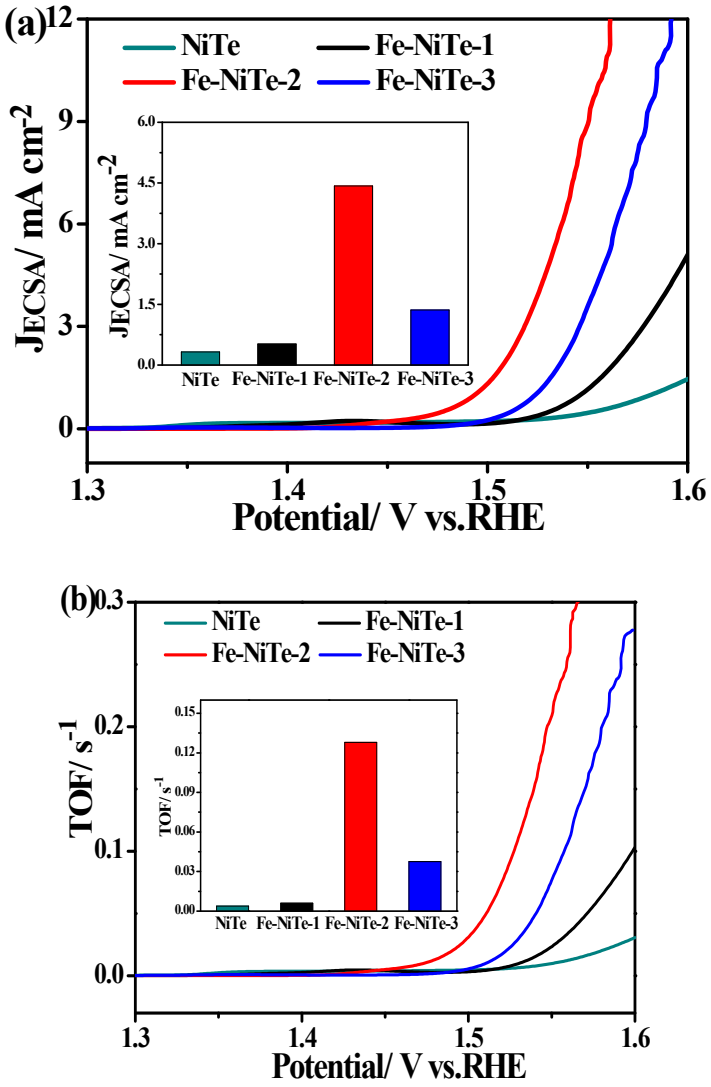

Fig. S6 (a) Specific activity of NiTe and Fe-doped NiTe at a scan rate of 5 mV s^{-1} in 1 M KOH solution by normalizing the raw current to the electrochemical surface areas. The inset shows the specific activity from the potential at ɳ =300 mV. (b) TOF value of NiTe and Fe-doped NiTe as a function of overpotentials. The inset shows the TOF value at η=300 mV.

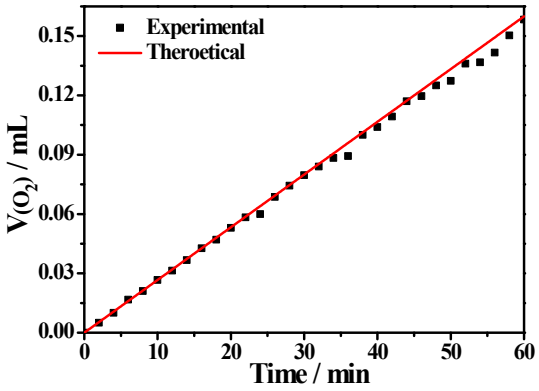

Fig. S7a Current efficiency for OER during constant voltage of 1.52 V vs. RHE in 1M KOH. The theoretical line represents the expected amounts of O_2 assuming a quantitative of nearly 100% Faradaic yield. The measured O_2 line represents the detected O_2.

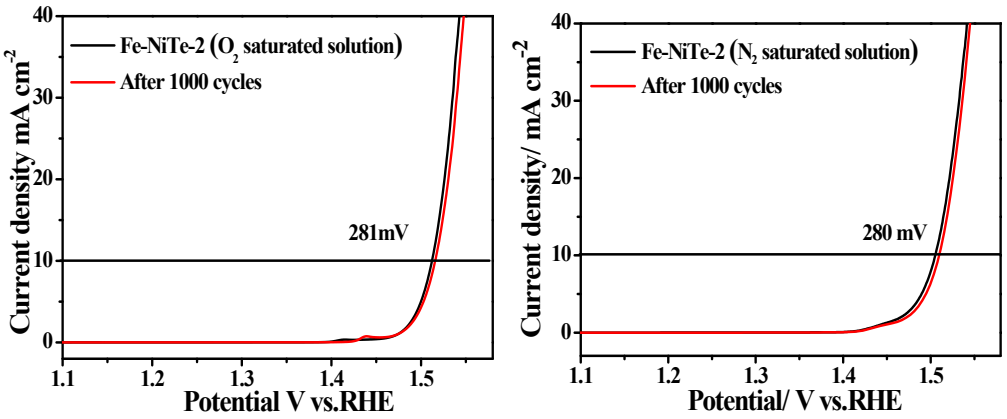

Fig. S7b Polarization curves of Fe-NiTe-2 before and after 1000 cycles with iR correction in O_2 and N_2 saturated 1 M KOH solution, respectively.

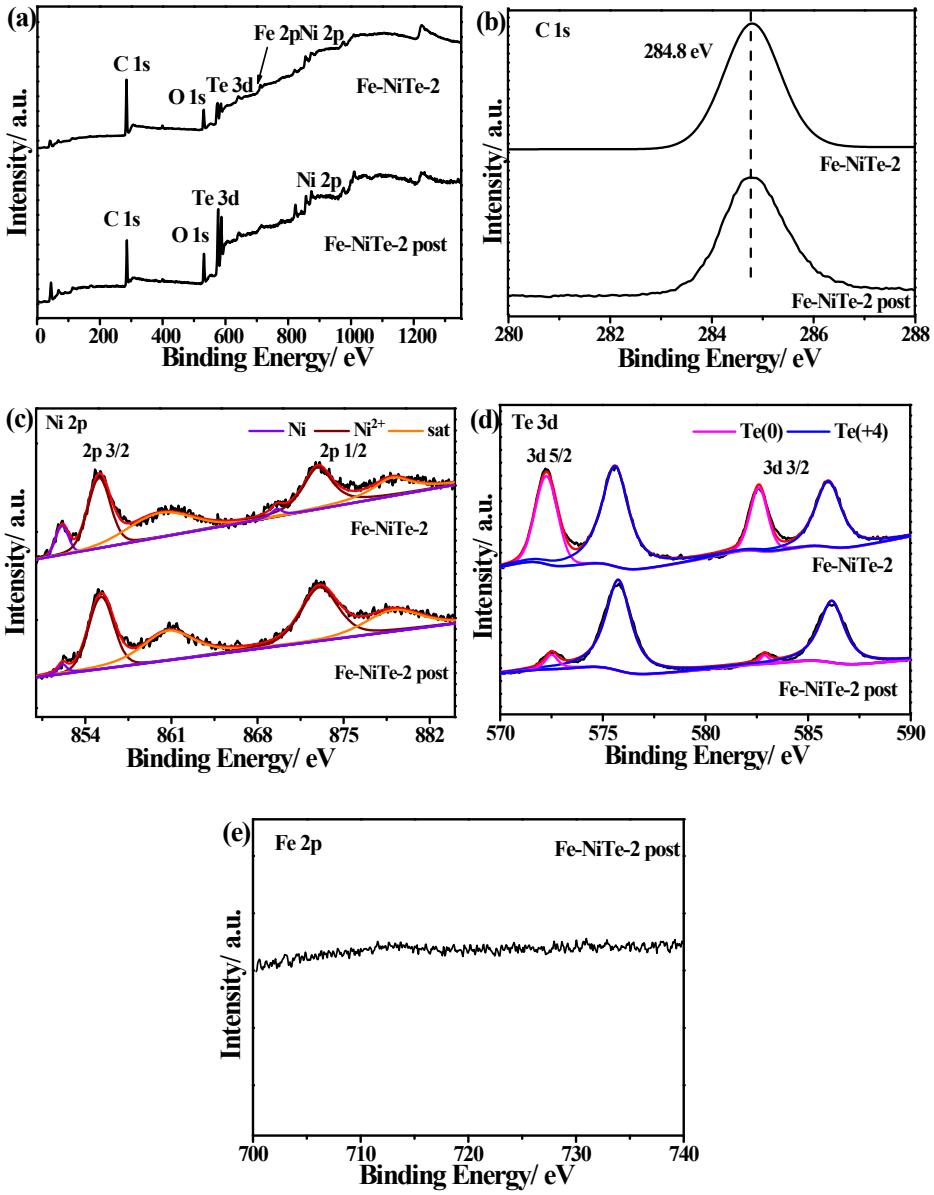

Fig. S8 XPS survey spectrum (a), high resolution XPS spectra of C 1s (b), Ni 2p (c), Te 3d (d) of Fe-NiTe-2 before and after OER electrolysis and Fe 2p (e) of Fe-NiTe-2 after OER electrolysis.

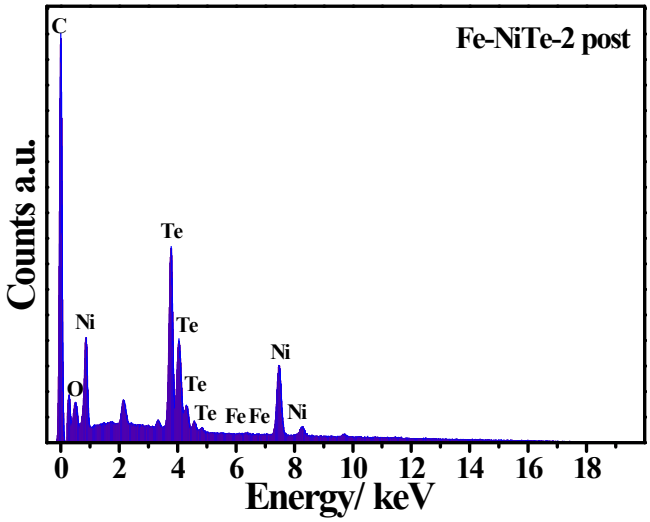

Fig. S9 EDS spectra of Fe-NiTe-2 after OER electrolysis.

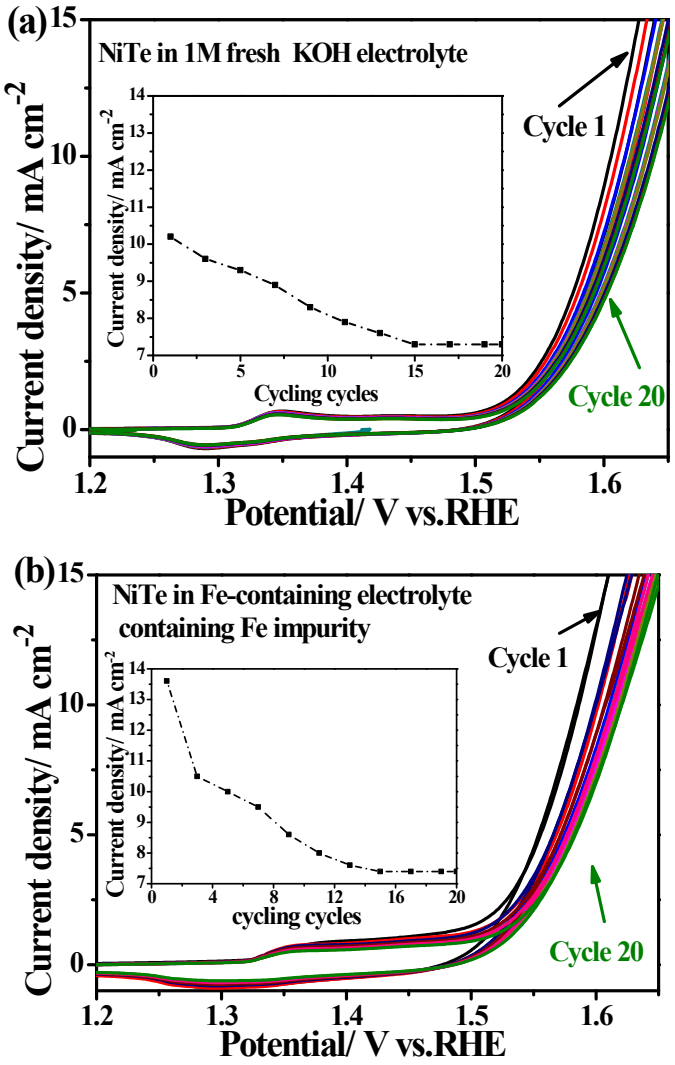

Fig. S10a-b Polarization curves (without iR correction) of NiTe in the fresh (a) and Fe-containing electrolyte (b) (inset for the current density at η=370 mV vs. Cycle numbers).

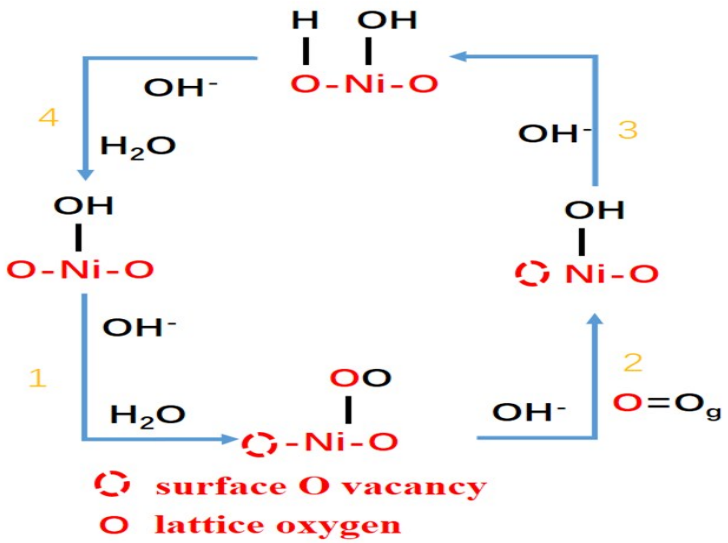

Fig. S10c Lattice oxygen mechanism of OER. The lattice oxygen mechanism follows the following pathway. Lattice oxygen can adsorb OH^- to form -OO and surface O vacancy, the adsorbed OO evolves back to -OH with the generation of O_2 (g). Once these occurs, the surface O vacancy becomes unstable, leading to a third step, in which OH^- (aq) fills the surface O vacancy and protonates an adjacent surface lattice oxygen. Finally, deprotonation take place, restoring the initial surface.[5]

Table S1. EDS analysis of Fe-doped NiTe catalysts.

Samples	Te	Ni	Fe
Fe-NiTe-1	53.0 at.%	46.8 at.%	0.2 at.%
Fe-NiTe-2	55.9 at.%	41.8 at.%	2.3 at.%
Fe-NiTe-3	43.6 at.%	50.8 at.%	5.6 at.%

Table S2. Binding energies of the Ni 2p 3/2 and Ni 2p 1/2 components for the Fe-NiTe-2 and NiTe catalysts.

Catalysts	Ni2p 3/2		Ni2p 1/2		
	Peak	Binding energy/ eV	Peak	Binding energy/ eV	Relatively content
Fe-NiTe-2	Ni(0)	852.1	Ni(0)	869.6	12.6%
	Ni(+2)	855.3	Ni(+2)	873.1	87.4%
NiTe	Ni(0)	851.9	Ni(0)	869.3	8.8%
	Ni(+2)	855.0	Ni(+2)	872.9	91.2%

Table S3. Binding energies of the Te 3d 5/2 and Te 3d 3/2 components for the Fe-NiTe-2 and NiTe catalysts.

Catalysts	Te3d 5/2		Te3d 3/2		
	Peak	Binding energy/ eV	Peak	Binding energy/ eV	Relatively Content
Fe-NiTe-2	Te(0)	572.3	Te(0)	582.6	35%
	Te(+4)	575.6	Te(+4)	586.0	65%
NiTe	Te(0)	572.4	Te(0)	582.8	50.5%
	Te(+4)	575.6	Te(+4)	586.0	49.5%

Table S4. Binding energies of the O 1s components for the Fe-NiTe-2 and NiTe catalysts.

Catalysts	Peak	Binding energy/ eV	Relatively content
Fe-NiTe-2	Metal O	529.5	13.4%
	Lattice O	530.5	49.0%
	Surface O	531.7	25.9%
	O in H_2O	533.2	11.7%
NiTe	Metal O	529.5	4.0%
	Lattice O	530.5	36.9%
	Surface O	531.7	38.0%
	O in H_2O	533.2	21.1%

Table S5. The comparison of other OER electrocatalysts in an alkaline electrolyte.

Catalysts	Electrolyte	Current density	Overpotential	Ref.
NiTe	1M KOH	10 mA cm^{-2}	388 mV	This work
Fe-NiTe-2	1M KOH	10 mA cm^{-2}	280 mV	This work
$CoTe_2$ nanoflecces	1M KOH	10 mA cm^{-2}	357 mV	[6]
$CoTe_2$@NCNTFs	1M KOH	10 mA cm^{-2}	330 mV	[7]
$NiCo_2O_4$	1M KOH	10 mA cm^{-2}	362 mV	[8]
NiO	1M KOH	10 mA cm^{-2}	360 mV	[9]
Fe-doped NiO	1M KOH	10 mA cm^{-2}	310 mV	[9]
$NiTe_2$/TM	1M KOH	10 mA cm^{-2}	315 mV	[10]
Ni_2P	1M KOH	10 mA cm^{-2}	340 mV	[11]
CoP	1M KOH	10 mA cm^{-2}	400 mV	[12]
NiS	1M KOH	10 mA cm^{-2}	320 mV	[13]

Table S6. EIS fitting parameters from equivalent circuits of NiTe and Fe-doped NiTe catalysts.

Catalysts	R_s	R_{ct}	R_0	CPE1/S s^{-n}	CPE2/S s^{-n}
NiTe	8.0	210.5	150.0	5.9E-5	4.3E-3
Fe-NiTe-1	7.8	85.7	62.0	4.4E-5	1.7E-4
Fe-NiTe-2	8.5	32.3	34.8	1.2E-5	1.2E-4
Fe-NiTe-3	7.9	51.4	50.5	3.3E-5	1.5E-4

Table S7a. Double layer capacitance (C_{dl}) and electrochemical surface area (ECSA) for NiTe and Fe-doped NiTe catalysts.

Samples	NiTe	Fe-NiTe-1	Fe-NiTe- 2	Fe-NiTe-3
C_{dl}/ mF cm^{-2}	0.197	0.202	0.242	0.226
ECSA/ cm^2	0.345	0.354	0.424	0.396

Table S7b. Specific activity and TOF values comparison of other OER electrocatalysts in 1M KOH electrolyte.

Catalyst	Overpotential	Specific activity	TOF values	Ref.
NiTe	300 mV	0.32 mA cm^{-2}	0.0038 s^{-1}	This work
Fe-NiTe-2	300 mV	4.4 mA cm^{-2}	0.13 s^{-1}	This work
$FeNi_3$/M-C-800	300 mV	0.24 mA cm^{-2}	0.11 s^{-1}	[14]
$(Ni,Fe)_3Se_4$	300 mV	0.13 mA cm^{-2}	0.043 s^{-1}	[15]
FeNi/SN-C-800	300 mV	0.25 mA cm^{-2}	0.063 s^{-1}	[16]
Fe-$NiSe_2$ (8.4%)	290 mV	-	0.071 s^{-1}	[17]
$Co_{0.7}Fe_{0.3}(OH)_x$	300 mV	-	0.022 s^{-1}	[18]

Table S8. Binding energy of the Ni 2p 3/2 and Ni 2p 1/2 components for the Fe-NiTe-2 before and after OER electrolysis.

Catalysts	Ni 2p 3/2		Ni 2p 1/2		
	Peak	Binding energy/ eV	peak	Binding energy/ eV	Relatively content
Fe-NiTe-2	Ni(0)	852.1	Ni(0)	869.6	12.6%
	Ni(+2)	855.3	Ni(+2)	873.1	87.4%
Fe-NiTe-2 post	Ni(0)	852.1	Ni(0)	869.5	0.3%
	Ni(+2)	855.2	Ni(+2)	873.0	99.7%

Table S9. Binding energies of the Te 3d 5/2 and Te 3d 3/2 components for the Fe-NiTe-2 before and after OER electrolysis.

Catalysts	Te3d 5/2		Te3d 3/2		
	Peak	Binding energy/ eV	Peak	Binding energy/ eV	Relatively Content
Fe-NiTe-2	Te(0)	572.3	Te(0)	582.6	35%
	Te(+4)	575.6	Te(+4)	586.0	65%
Fe-NiTe-2 post	Te(0)	572.5	Te(0)	582.8	6.5%
	Te(+4)	575.7	Te(+4)	586.1	93.5%

Table S10. Binding energies of the O 1s components for Fe-NiTe-2 before and after OER electrolysis.

Catalysts	Peak	Binding energy / eV	Relatively content
Fe-NiTe-2	Metal O	529.5	13.4%
	Lattice O	530.5	49.1%
	Surface O	531.7	25.9%
	O in H_2O	533.2	11.6%
Fe-NiTe-2 post	Metal O	529.5	19.5%
	Lattice O	530.4	54.5%
	Surafce O	531.7	22.0%
	O in H_2O	533.2	4.0%

Table S11. EDS analysis of Fe-NiTe-2 catalysts and Fe-NiTe-2 before and after OER electrolysis.

Samples	Te	Ni	Fe
Fe- NiTe-2	55.9 at.%	41.8 at.%	2.3 at.%
Fe-NiTe-2 post	53.0 at.%	46.9 at.%	0.1 at.%

References

1. L. Yang, L. Chen, D. Yang, X. Yu, H. Xue and L. Feng, *J. Power Sources*, 2018, **392**, 23-32.
2. Y. Wang, Z. Liu, H. Liu, N. T. Suen, X. Yu and L. Feng, *ChemSusChem*, 2018, **11**, 2724-2729.
3. J.-X. Feng, J.-Q. Wu, Y.-X. Tong and G.-R. Li, *J. Am. Chem. Soc.*, 2018, **140**, 610-617.
4. Z. Pu, Q. Liu, A. M. Asiri and X. Sun, *ACS Appl. Mater. Interfaces*, 2014, **6**, 21874-21879.
5. X. Rong, J. Parolin and A. M. Kolpak, *ACS Catal.*, 2016, **6**, 1153-1158.
6. Q. Gao, C. Q. Huang, Y. M. Ju, M. R. Gao, J. W. Liu, D. An, C. H. Cui, Y. R. Zheng, W. X. Li and S. H. Yu, *Angew. Chem.-Int. Edit.*, 2017, **56**, 7769-7773.
7. X. Wang, X. Huang, W. Gao, Y. Tang, P. Jiang, K. Lan, R. Yang, B. Wang and R. Li, *J. Mater. Chem. A*, 2018, **6**, 3684-3691.
8. X. Ding, Y. Huang and M. Zong, *Mater. Lett.*, 2015, **157**, 285-289.
9. A. C. Pebley, E. Decolvenaere, T. M. Pollock and M. J. Gordon, *Nanoscale*, 2017, **9**, 15070-15082.
10. Z. Wang and L. Zhang, *ChemElectroChem*, 2018, **5**, 1153-1158.
11. H. Sun, X. Xu, Z. Yan, X. Chen, F. Cheng, P. S. Weiss and J. Chen, *Chem. Mater.*, 2017, **29**, 8539-8547.
12. M. Liu and J. Li, *ACS Appl. Mater. Interfaces*, 2016, **8**, 2158-2165.
13. P. Luo, H. Zhang, L. Liu, Y. Zhang, J. Deng, C. Xu, N. Hu and Y. Wang, *ACS Appl. Mater. Interfaces*, 2017, **9**, 2500-2508.
14. Z. Liu, X. Yu, H. Yu, H. Xue and L. Feng, *ChemSusChem*, 2018, **11**, 2703-2709.
15. J. Du, Z. Zou, C. Liu and C. Xu, *Nanoscale*, 2018, **10**, 5163-5170.
16. Z. Liu, H. Yu, B. Dong, X. Yu and L. Feng, *Nanoscale*, 2018, **10**, 16911-16918.
17. C. Gu, S. Hu, X. Zheng, M. R. Gao, Y. R. Zheng, L. Shi, Q. Gao, X. Zheng, W. Chu, H. B. Yao, J. Zhu and S. H. Yu, *Angew. Chem. Int. Ed.*, 2018, **57**, 4020-4024.
18. T. Zhou, Z. Cao, H. Wang, Z. Gao, L. Li, H. Ma and Y. Zhao, *RSC Advances*, 2017, **7**, 22818-22824.